An Investigation of Dynamic Response of 19 Passenger Commuter Aircraft Windshield against Bird Strike

Budi Aji Warsiyanto[1], Abian Nurrohmad[2], Rizky Fitriansyah[3], Agus Bayu Utama[4], Sahril Afandi Sitompul[5], Endah Yuniarti[6]

[1,5,6]Faculty of Aerospace Technology, Air Marshal Suryadarma University, Indonesia

[2,3,4]Aerostructural Laboratory, National Institute of Aeronautics and Space (LAPAN), Indonesia

[1]e-mail: budiajiwarsiyanto@gmail.com

Received: 14-03-2021. Accepted: 04-08-2021. Published: 30-12-2021

Abstract

This research renders a numerical investigation of a 19 passenger commuter aircraft windshield subjected to bird strike impact. The objective of this research was to determine the dynamic response of a 19 passenger commuter aircraft windshield to impact angle variations. The phenomenon was performed using the finite element method, and the smoothed particle hydrodynamics (SPH) was chosen as a method for modeling bird material. A gelatin material was employed as the bird model and the elastic-plastic polymethyl methacrylate (PMMA) material with the maximum principal strain failure criterion was employed to model the windshield's dynamic response. As most bird strikes occur during take-off and landing, the bird was modeled with an initial velocity of 62 m/s and is impacted on the windshield, where the damage of the windshield is then assessed. The windshield was modeled as a hexahedron mesh for accuracy in finite element software and is fixed at the edge. The variation of the impact angle consists of 15°, 0°, -8°, and -15°, which are measured of the longitudinal axis of the aircraft. The simulation result showed that the impact angle that causes the windshield's dynamic response in the elastic, plastic deformation, and the greatest failure is the angle -15°. The upper end of the windshield (fixed) is the weakest part due to the stress concentration.

Keywords*: Bird strike; dynamic response, windshield; PMMA, finite element.*

Nomenclature

L	=	length of the bird, m
D	=	the diameter of bird, m
P_S	=	stagnation pressure, MPa
P_H	=	Hugoniot pressure, MPa
ρ	=	density, kg/m^3
v	=	impact velocity, m/s
ε	=	strain, -
σ	=	stress, MPa
E	=	elastic modulus, MPa
ν	=	poisson's ratio, -
$f(\varepsilon_{vol})$	=	functions of the logarithmic volumetric strain
E_m	=	internal energy per unit mass

1. Introduction

Commuter flights will still be a mainstay of Indonesia to open isolation in remote areas, both in the mountains and small islands. This is due to the large number of remote

areas in Indonesia that have very short aircraft runways. One of the categories of aircraft included in pioneer flights is commuter aircraft. Based on CASR part 23, the commuter category is limited to propeller-driven, multiengine airplanes that have a seating configuration, excluding pilot seats, of 19 or less, and a maximum certificated takeoff weight of 19,000 pounds or less (Republic Indonesia Ministry of Transportation, 2014).

The test requirements refer to the Civil Aviation Safety Regulation (CASR) part 23 issued by the Ministry of Transportation of the Republic of Indonesia. One of the tests performed to obtain certification is the strength of the aircraft's structure and components when it receives loads due to bird strikes. Based on CASR subpart 23.775, windshield panes directly in front of the pilots in the normal conduct of their duties, and the supporting structures for these panes, must withstand, without penetration, the impact of a two-pound bird when the velocity of the airplane (relative to the bird along the airplane's flight path) is equal to the airplane's maximum approach flap speed (Republic Indonesia Ministry of Transportation, 2014).

Based on the Federal Aviation Administration (FAA) data, from 2015 to 2019, there has been a bird strike phenomenon of more than 60,663 times. Bird strikes often occur at altitudes of less than 3,000 feet (914.4 meters) with a percentage of 95% (FAA, 2019). Therefore, take-off, approach, and landing become critical flight phases in a bird strike phenomenon (Shahimi et al., 2021). Components of fixed-wing aircraft with the potential to sustain bird strikes are shown in Figure 1. However, in helicopters, components that can sustain bird strikes include windshields, fuselage panels, and rotor blades (R. Hedayati et al., 2014). Although aircraft components also can sustain attacks from other objects or Foreign Object Damage (FOD), 90% of damage is caused by bird strikes (Heimbs, 2011b).

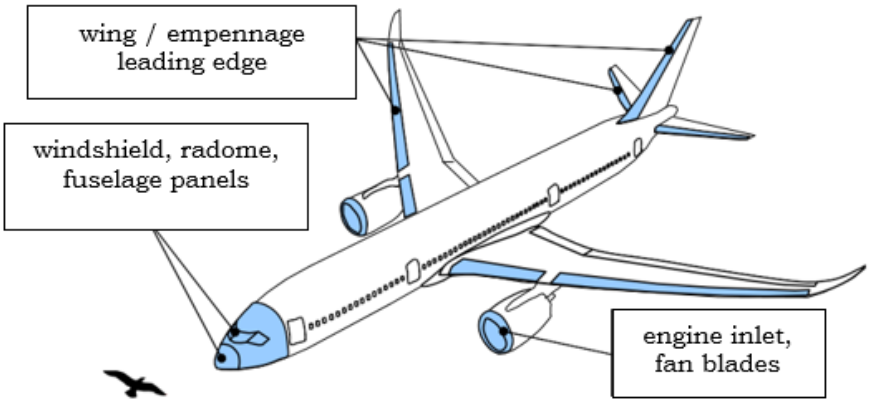

Figure 1: Components of a plane that has the potential to sustain bird strike (Heimbs, 2011a)

Experiments are the best method to analyze bird strikes realistically. However, this method is less effective (cannot give repeatable results due to bird species differences) and less efficient (requires time and cost in the target-making process). In 1970, a more effective and efficient method was found, namely numerical software (finite element) application (Reza Hedayati & Sadighi, 2015). In this study, a bird strike simulation was performed to determine a 19 commuter aircraft windshield dynamic response based on variations in the impact angle. In this study, simulations were performed using Abaqus finite element software. As most bird strikes occur during take-off and landing, the bird was modeled with an initial velocity of 62 m/s and is impacted on the windshield, where the damage of the windshield is then assessed.

2. Methodology

2.1. Related Works

Several researchers, such as (Zhu et al., 2009) have investigated windshield responses to bird strikes using experimental and numerical methods, (X. Wang et al., 2007), (F. S. Wang & Yue, 2010), and (Dar et al., 2013) simulate the failure of the windshield with polymethyl methacrylate (PMMA) material against bird strike. (Yuniarti & Sitompul, 2019)

analyzes the effect of a cylindrical and hemispherical-cylinder bird model using the lagrangian method. The analysis of bird mass variation to determine a 19 commuter aircraft windshield dynamic response has been performed by (Warsiyanto, Nurrohmad, et al., 2020). In addition, the analysis of impact velocity variation and difference of thickness of a 19 commuter aircraft windshield dynamic response has been performed by (Warsiyanto, Sitompul, et al., 2020).

2.2. Problem Definition

If the windshield fails, it creates a dangerous condition for two reasons: first, when the bird passes through the windshield, it can enter the cockpit and collide with the pilot's head. This collision can cause the pilot to become incapacitated and then the downing of the aircraft. Second, the windshield itself can collide with the pilot's head while moving rapidly downward. Therefore, this research aims to see the dynamic response of the PMMA windshield structure to the impact angle variation so that critical conditions can be obtained and can anticipate damage to the windshield.

2.3. Method

The phenomenon of bird strike impact was performed using the finite element method, namely the Abaqus CAE software. The SPH was chosen as a method for modeling bird material because enables large deformations and splitting of the bird model without additional care. This method can be coupled to the Finite Element (FE) solution typically employed for the structural models using a penalty contact algorithm since both methods are based on the Lagrangian formulation (Siemann & Ritt, 2019). The SPH method is widely used to simulate the bird as it has been proven that SPH can reproduce the main physical effects of the bird-strike phenomenon (Heimbs et al., 2015). SPH is a mesh-free numerical method; therefore, the bird model is discretized with particles that are not interconnected as in the mesh-based method. According to (Heimbs, 2011b), SPH has more advantages than other bird modeling methods (eulerian and lagrangian). The elastic-plastic polymethyl methacrylate (PMMA) material with the maximum principal strain failure criterion was used to model the windshield's dynamic response. The impact angle differences consist of 15°, 0°, -8°, and -15°, which are measured of the longitudinal axis of the aircraft with an impact velocity of 62 m/s and bird mass of 0.91 kg (2 lb).

2.4. Validation of Numerical Model

The validation of numerical modeling was performed by simulating impacts between bird and plate. The plate was given the linear isotropic material model of steel with a density of 7800 kg/m3, Young Modulus of 207 GPa, and Poisson's ratio of 0.3 (Reza Hedayati & Ziaei-Rad, 2013). The bird's dimensions are according to the sabot's size (bird container) on the PUSTEKBANG LAPAN bird strike test equipment. The geometry is shown in Figure 2-1 (a) with a length (L) of 74 mm and a diameter (D) of 129 mm. Bird model is converted to particles (characteristic of the SPH method) as shown in Figure 2-1 (b) with 6741 particles. The plate is modeled as a square with 1000 mm, supported (fixed) on each side. A gelatin material was employed as the surrogate bird material model. The material properties of the gelatin are shown in Table 2-1. In addition, the approach uses the tabulated equation of state representation to input directly the Hugoniot curves for water-like homogenized bird materials with various of porosity given by Eq. (2-1) (see Figure 2-2).

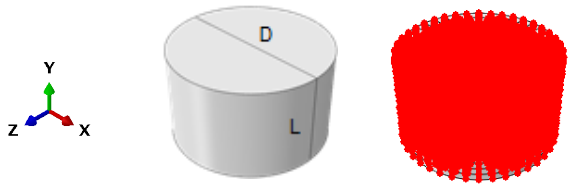

(a) (b)

Figure 2-1: (a) Geometry and (b) particle model of bird

The results are compared with the results of analytics and experiments conducted by (Wilbeck, 1978). Birds are modeled by the SPH method and are impacted into steel plates at a velocity of 200 m/s. The deformation stage of the bird is shown in Figure 2-3. The peak pressure (P_H) values were obtained from the center point on the plate.

Table 2-1: A gelatin mechanical properties (SIMULIA, 2011)

Density (kg/m³)	Shear modulus (MPa)	Yield strength (MPa)	Elastic strain	Hydrostatic strength (MPa)	Initial failure
938	10	0.1	0.01	2.75	4 ε_{el}

$$P_H = f_1(\varepsilon_{vol}) + \rho_0 f_2(\varepsilon_{vol}) E_m \quad (2\text{-}1)$$

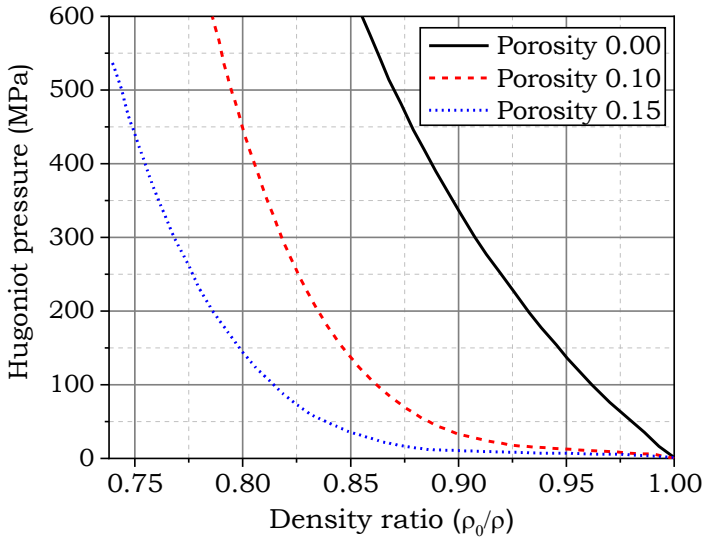

Figure 2-2: Hugoniot pressure to density ratio curves for bird material (SIMULIA, 2011)

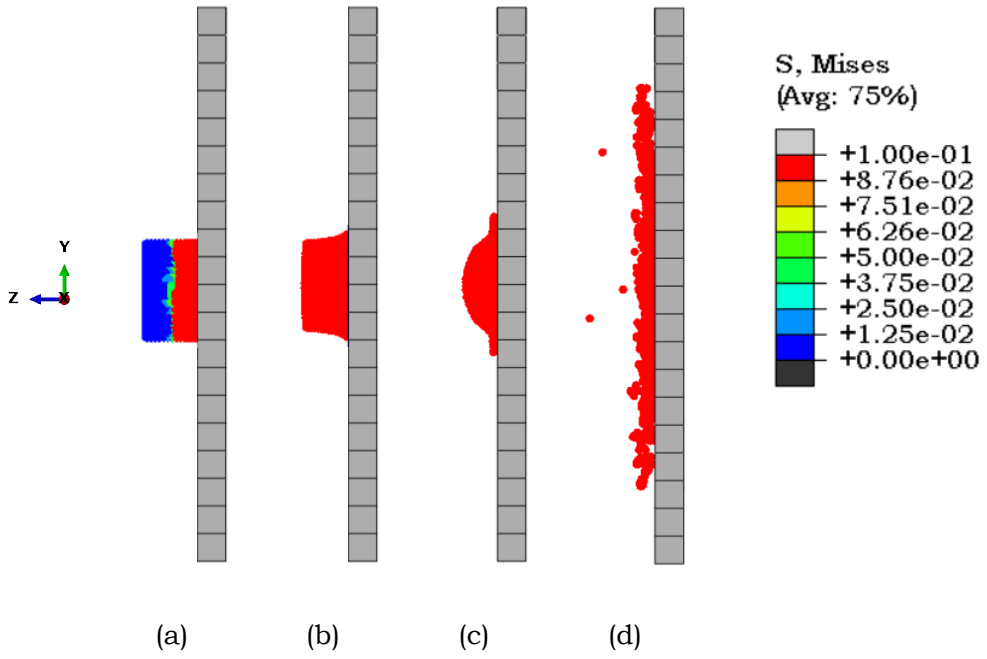

Figure 2-3: Deformation of a bird on impacting a steel plate based on time interval, (a) 0.02 ms, (b) 0.06 ms, (c) 0.22 ms, and (d) 1 ms

Simulation results are shown with a normalized pressure. Normalization of pressure was performed by dividing the value of numerical pressure with an analytical stagnation pressure (P_S), while normalizing time was performed by dividing the numerical time value by analytical time (t). Stagnation pressure and time can be calculated by using the equation as follows (Wilbeck, 1978):

$$P_S = \frac{1}{2}\rho v^2 \tag{2-1}$$

$$t = \frac{l}{v} \tag{2-2}$$

For numerical simulations, the peak pressure has a value of 361.93 MPa, so that it gives a normalization value of 19.29. For the experiment, the peak pressure has a value of 340.19 MPa, so that it gives a normalization value of 18.13. For analytical, the peak pressure has a value of 353.23 MPa, so that it gives a normalization value of 18.83. A comparison of numerical, analytical, and experimental methods is shown in Figure 2-4. Based on Figure 2-4, the trend of the plot is consistent with the experimental result. It appears that the peak pressure occurs at the initial of the impact and then stabilized with time. In addition to this, the duration of pressure decay was also following the experimental result.

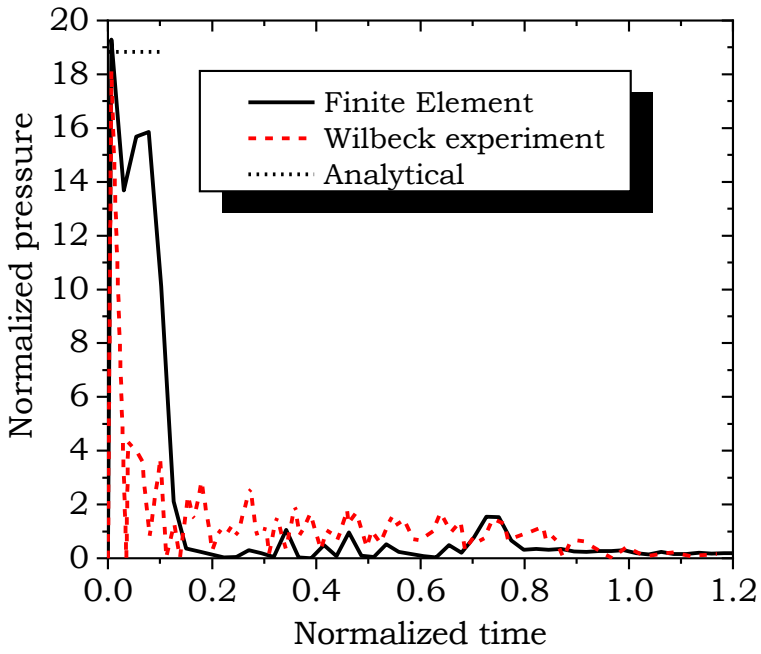

Figure 2-4: Comparison pressure profile between finite element, experimental, and analytical result

In addition to validating the bird model, the windshield model also needs to be validated using the Mesh convergence method. Based on (Abaqus, 2014), the coarse mesh can give inaccurate results, so that is recommended to use fine mesh. Consequently, the required computer specifications will increase when the mesh is refined. However, this can be overcome by fine mesh only in certain areas. The effect of differences in mesh size is considered based on maximum displacement at the center of impact location on the windshield, as shown in Figure 2-5. It is found that the mesh size per element that produces convergent values is 10 - 5 mm, with the number of elements ranging from 16144 - 57518.

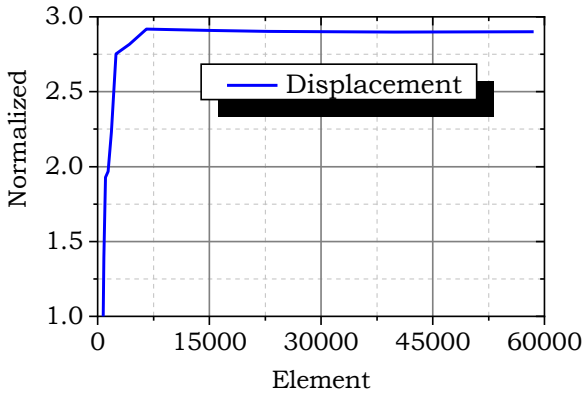

Figure 2-5: Convergence results in mesh comparisons

2.5. Numerical Modeling

The material for the windshield model is polymethyl methacrylate (PMMA). The mechanical properties of PMMA are shown in Table 2-2. The bird strike scenario on the 19 passengers commuter aircraft windshield is shown in Figure 2-6. The different scenarios for the angle of impact on the aircraft's longitudinal axis are shown in Figure 2-7. Location 1 was chosen as a reference for data output (displacement and force) because it is the farthest area from the supporting structure and directly faces the pilot in carrying out his duties.

Table 2-2: Material properties of the windshield (Dar et al., 2013)

Density (kg/m³)	Young modulus (GPa)	Poisson's ratio	Yield strength (MPa)	Ultimate strength (MPa)	Failure strain
1186	3.2	0.4	68	78	0.067

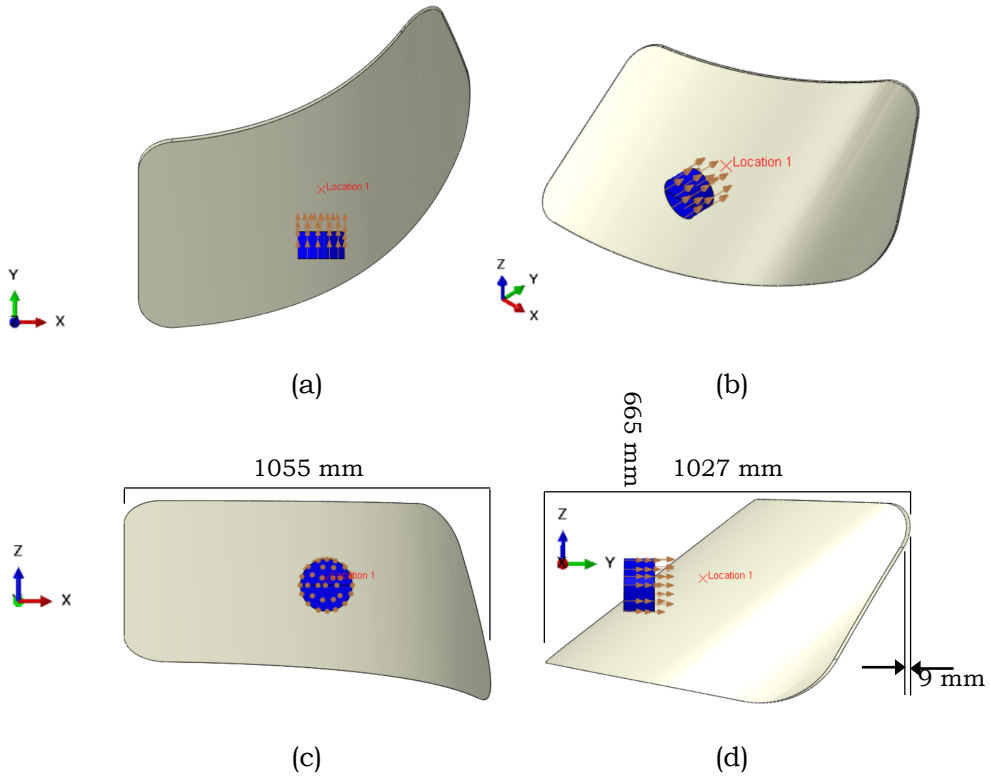

Figure 2-6: Bird strike on the windshield: (a) upper, (b) isometric, (c) front, and (d) side view

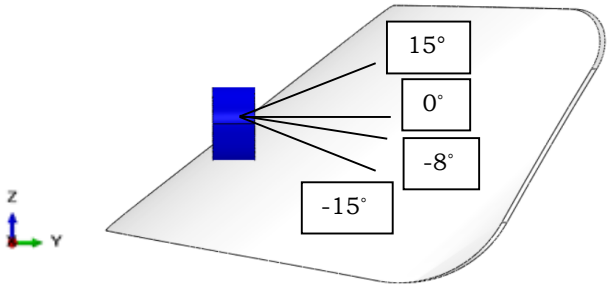

Figure 2-7: Different impact angle

The simulation time of 0.02 seconds was chosen because it considers the bird's effect on the overall dynamic response of the windshield. The contact type is General contact (Explicit) because it represents the entire model for analysis. In addition, this type is suitable for interactions between particles (birds) and elements (targets) (Abaqus, 2014).

Velocity is the loading parameter applied to the bird model that is showed by the arrow in Figure 2-8. Boundary conditions were applied to the windshield's edge because the windshield is supported by a supporting structure at the edge that holds the translational and rotational displacement of the three x, y, and z axes.

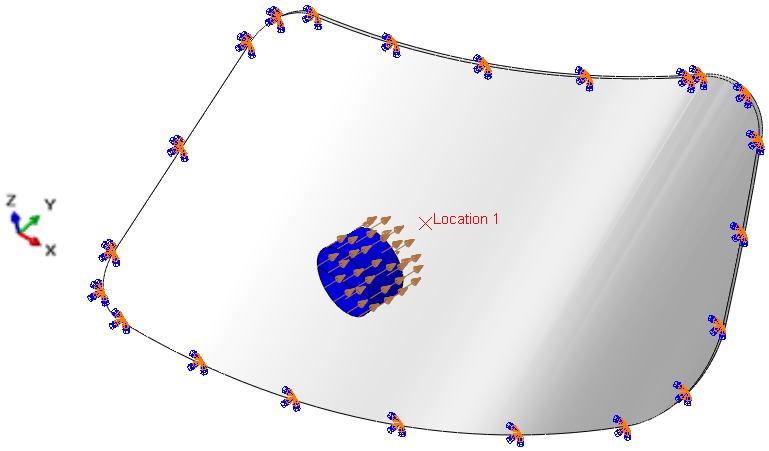

Figure 2-8: Load and boundary conditions on the windshield models

Based on the convergence mesh results, mesh size per element for windshield ranges from 10 - 5 mm (Figure 2-9). A size of 5 mm was employed on the impact area along with the bird's contact. The windshield mesh consists of 27686 elements.

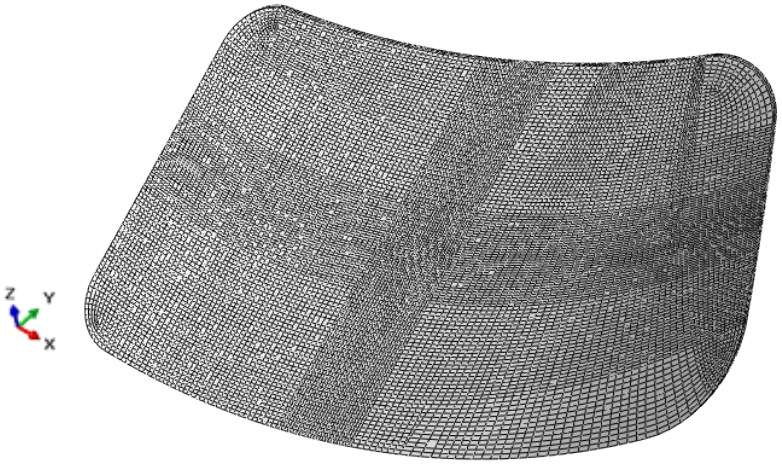

Figure 2-9: Mesh of windshield model

3. Result and Analysis

Simulations were performed at an impact velocity of 62 m/s and bird mass of 0.91 kg as fixed parameters. Figure 3-1(a) shows the more normal angle of impact against the windshield (15° to -15°) causing an increase in maximum displacement. To provide complete and comprehensive knowledge, the displacement vs. time for variations in impact velocity and bird mass are shown in Figure 3-1(b) (Warsiyanto, Sitompul, et al., 2020) and Figure 3-1(c) (Warsiyanto, Nurrohmad, et al., 2020), respectively. It can be seen that the greatest displacement at the impact velocity variations occurs in the 87.5 m/s. The displacement curve at the impact velocity of 87.5 m/s did not decrease completely because the windshield failed (penetration). In addition, the greatest displacement of the bird mass variation occurs in the 1.81 kg of scenario. Similar to the impact velocity variation, the displacement curve for the 1.81 kg bird mass variation did not decrease completely because the windshield failed.

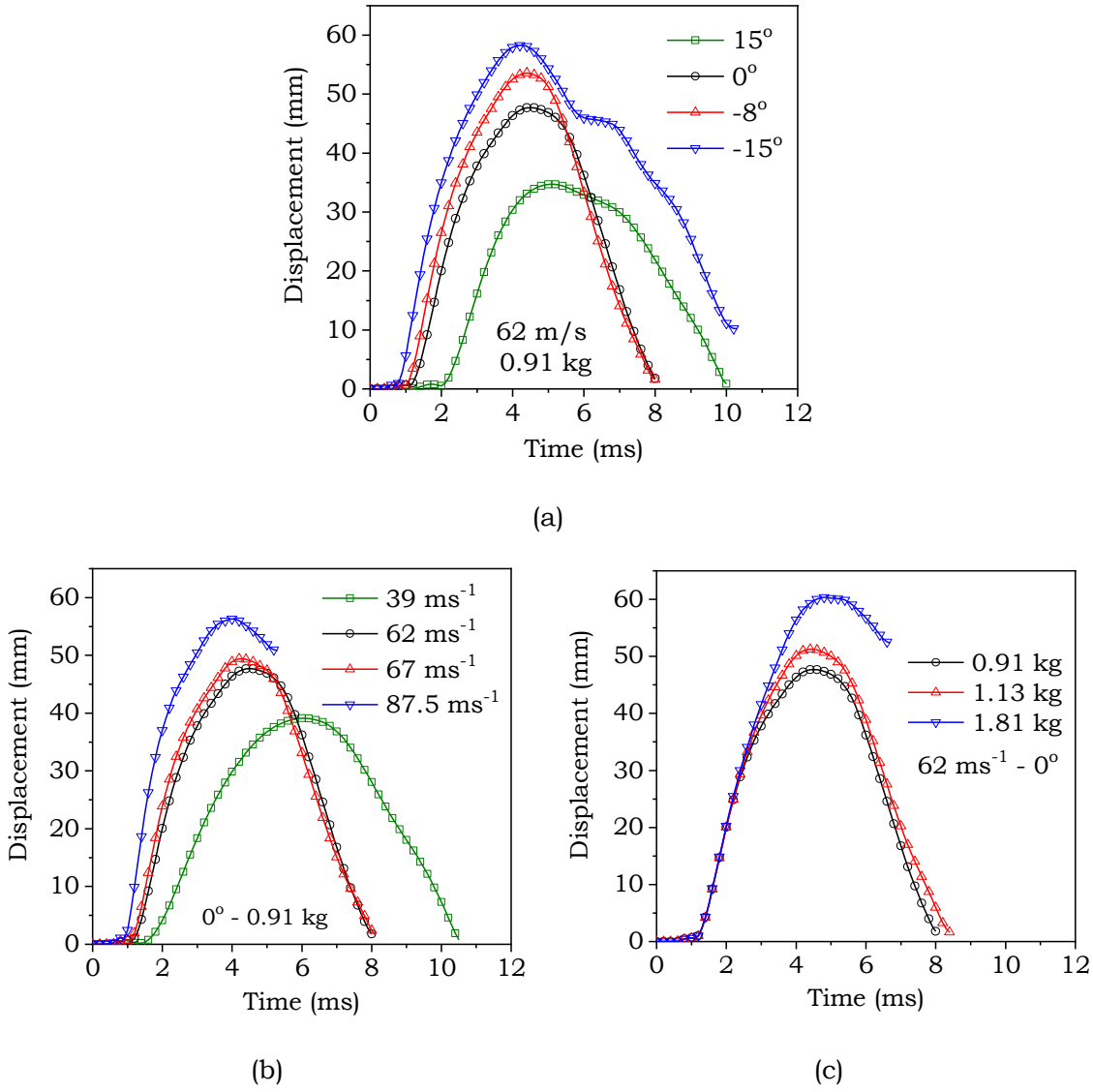

Figure 3-1: Displacement vs. time plot based on impact parameters variation: (a) impact angle, (b) impact velocity (Warsiyanto, Sitompul, et al., 2020), and (c) bird mass (Warsiyanto, Nurrohmad, et al., 2020)

Figure 3-2(a) shows the impact force that increases with the normal angle of impact against the windshield. At an angle of 15°, the peak force that occurs is 25.12 N at 4.3 ms and increases to 84.15 N at 1.3 ms for an angle of -15°. There is an increase in peak force by three times in the different impact angles from 15° to -15°. To provide complete and comprehensive knowledge, the force vs. time for variations in impact velocity and bird mass are shown in Figure 3-2(b) (Warsiyanto, Sitompul, et al., 2020) and Figure 3-

2(c) (Warsiyanto, Nurrohmad, et al., 2020), respectively. It can be seen that at a velocity of 39 ms^{-1}, the maximum impact force of 16.72 N is recorded at 4 ms which rises to 102.77 N at 1 ms for a velocity of 87.5 ms^{-1}. An increase of 6 times in maximum impact force was observed due to a change in impact velocity from 39 ms^{-1} to 87.5 ms^{-1}. In addition, at a bird mass of 0.91 kg, the maximum impact force of 43.42 N is recorded at 1.9 ms which rises to 71.67 N at 4.1 ms for 1.81 bird mass. An increase of 1.7 times in maximum impact force was observed due to a change in bird mass from 0.91 kg to 1.81 kg.

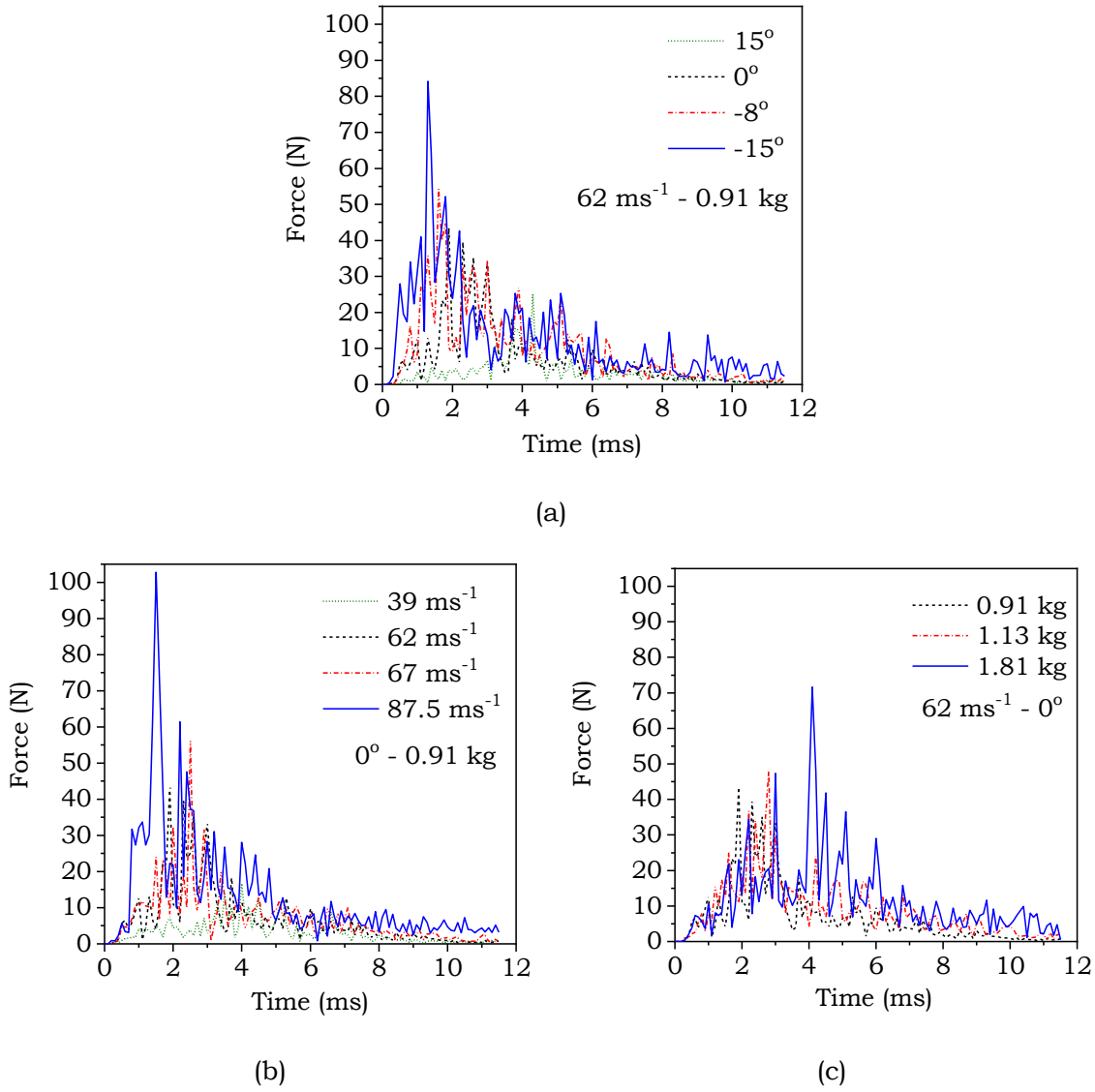

Figure 3-2: Impact force history for different impact angles

Figure 3-3 shows the stress distribution on the windshield. The more normal impact angle of birds against windshield (15° to -15°) causes a wider distribution of stress. This is caused by the increase in the impact force so that the stress flow will spread wider until the value of the force decreases. At an angle of 0°, -8°, and -15°, the maximum stresses are 77.46, 77.98, and 77.98 MPa, respectively. The stress value is almost the same as the maximum material stress, namely 78 MPa. For each impact angle, a stress concentration occurs at the upper and lower ends of the windshield which is indicated to be the initial location of the failure.

The stress distributions on the windshield for different impact velocity and bird mass are shown in Figure 3-4 (Warsiyanto, Sitompul, et al., 2020) and Figure 3-5 (Warsiyanto, Nurrohmad, et al., 2020), respectively. At all impact velocity and bird mass, the stress that occurs at the upper end of the windshield has exceeded the yield strength of the material (68 MPa) even almost equals to the maximum stress material (78 MPa). There is

a stress concentration at the upper and lower end of the windshield which is indicated to be the initial location of the failure. However, the stress concentration at the upper end is more dominant than the lowermost because birds tend to move to the upper end region (the vector between positive y and z axes) in all scenarios.

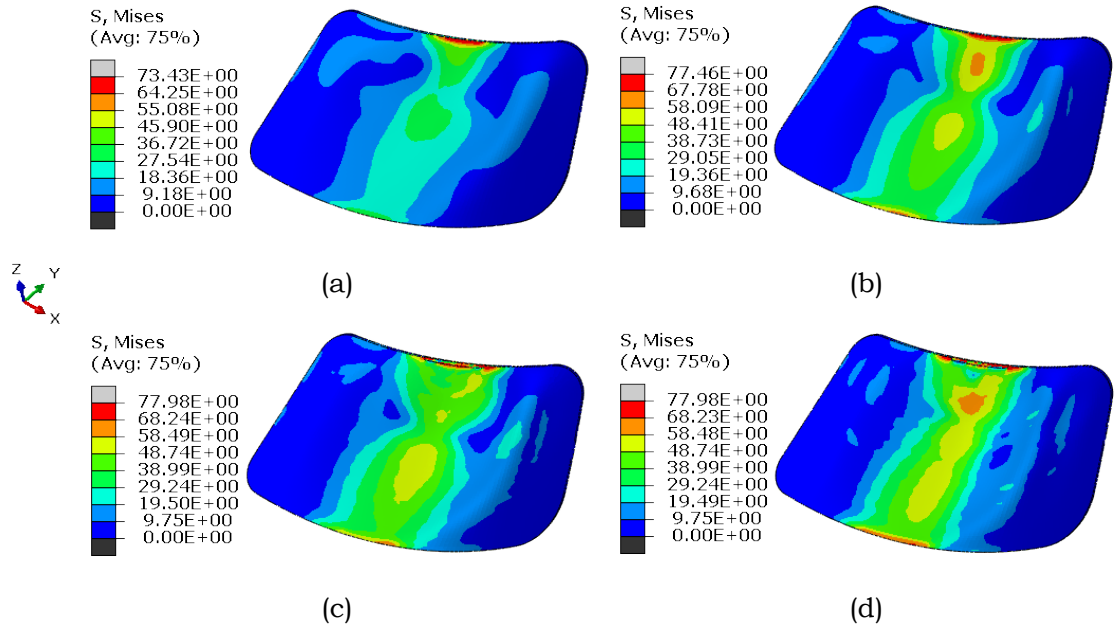

Figure 3-3: Stress distribution on the windshield for impact angle variations: (a) 15°; (b) 0°; (c) -8°; and (d) -15°

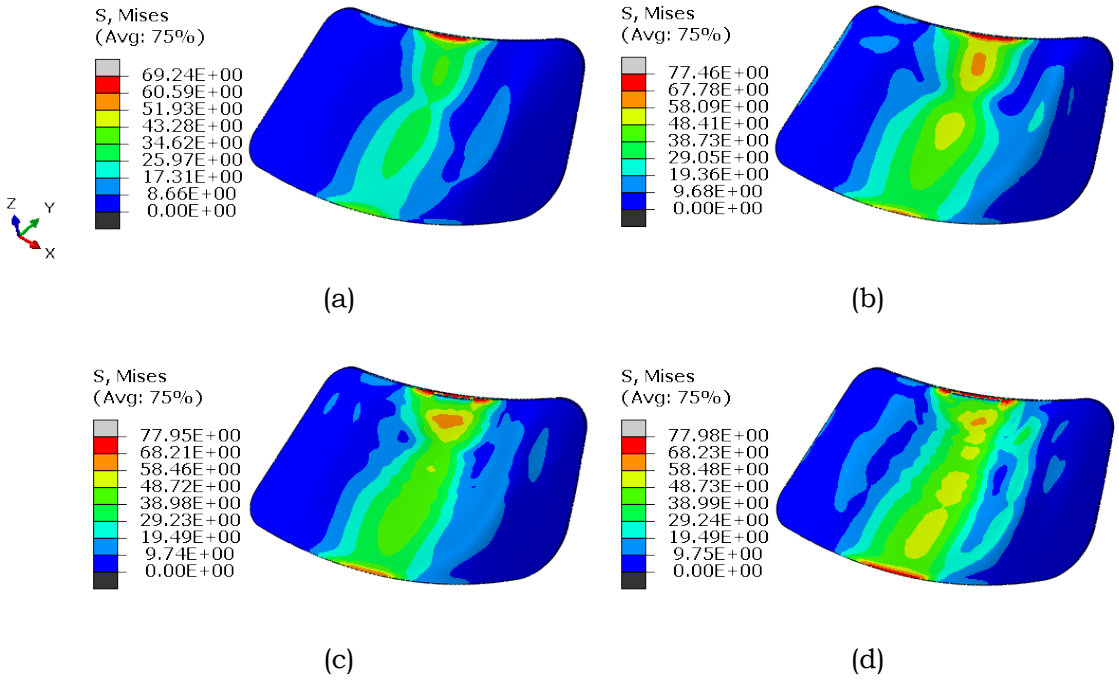

Figure 3-4: Stress distribution on the windshield for impact velocity variations: (a) 39; (b) 62; (c) 67; and (d) 87.5 m/s (Warsiyanto, Sitompul, et al., 2020)

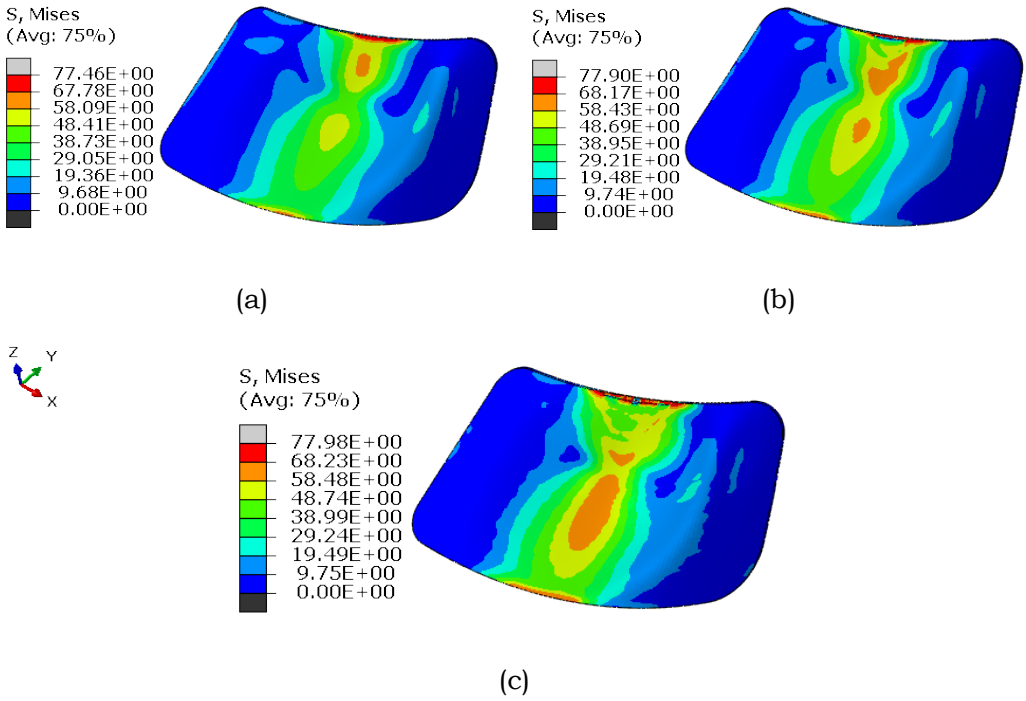

Figure 3-5: Stress distribution on the windshield for bird mass variations: (a) 0.91; (b) 1.13; (c) 1.81 kg (Warsiyanto, Nurrohmad, et al., 2020)

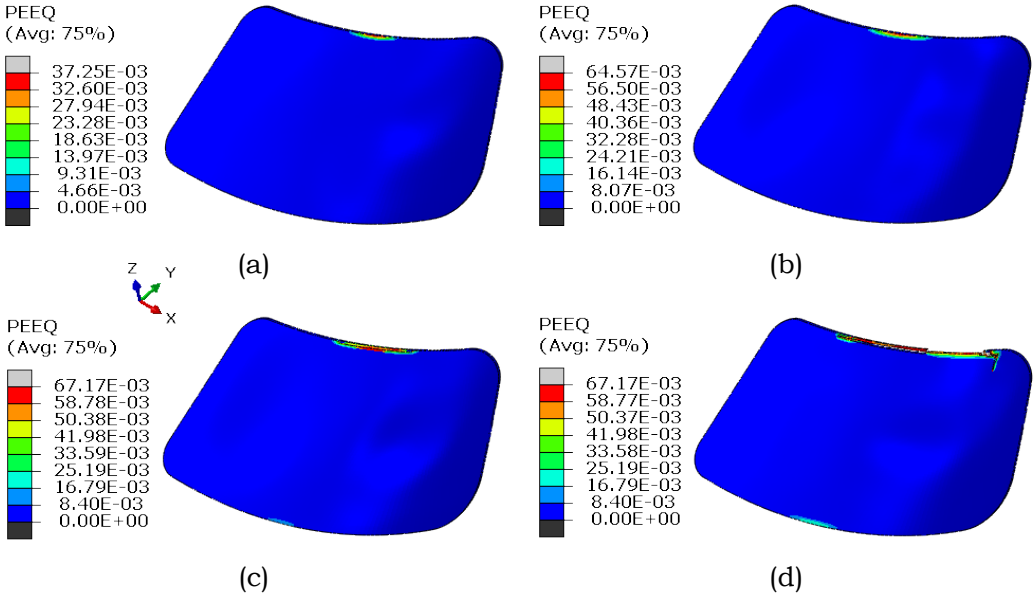

Figure 3-6: Plastic strain area on the windshield for impact angle variations: (a) 15°, (b) 0°, (c) -8°, and (d) -15°

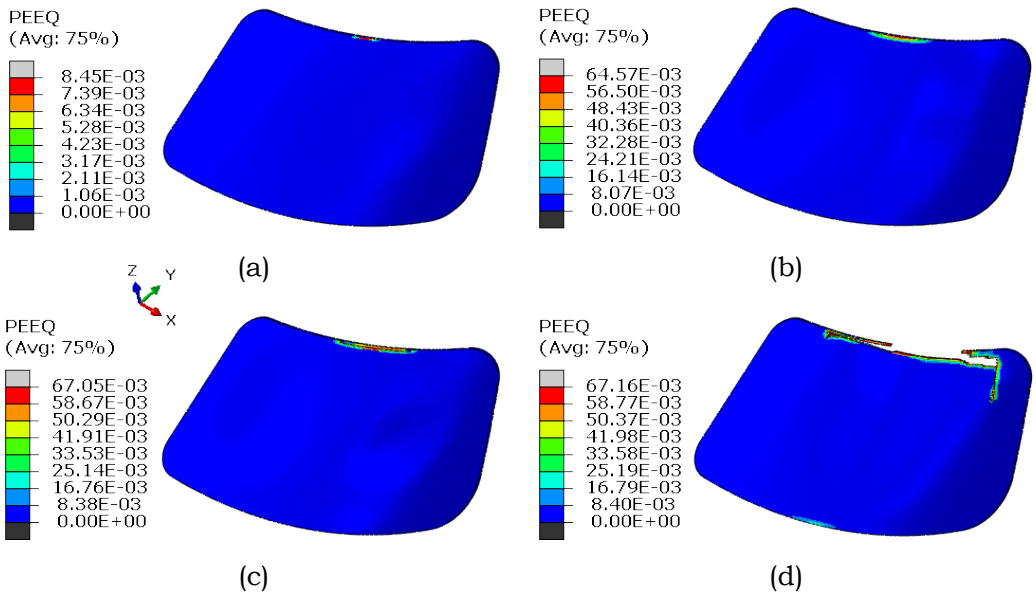

Figure 3-7: Plastic strain area on the windshield for impact velocity variations: (a) 39 m/s, (b) 62 m/s, (c) 67 m/s, and (d) 87.5 m/s (Warsiyanto, Sitompul, et al., 2020)

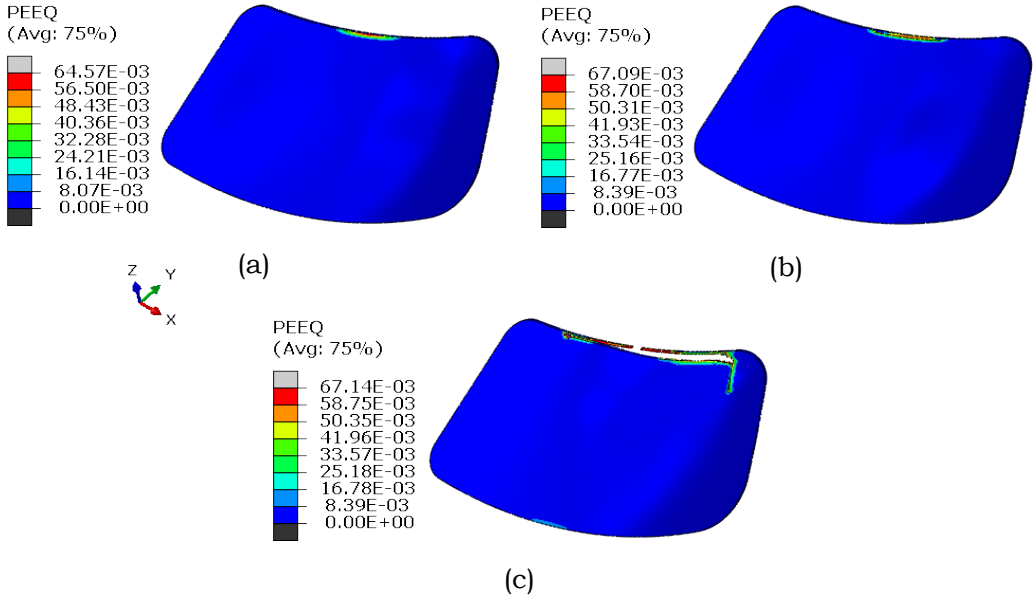

Figure 3-8: Plastic strain area on the windshield for bird mass variations: (a) 0.91 kg, (b) 1.13 kg, and (c) 1.81 kg (Warsiyanto, Nurrohmad, et al., 2020)

The plastic strain area of the windshield extends as the normal angle of impact as shown in Figure 3-6. The plastic strain occurs in all impact angles at the upper end of the windshield which indicates stresses exceeding the yield strength of the material. The windshield begins to crack (local failure) at the upper end at an impact angle of -8° which is considered a critical factor. When the impact angle exceeds -8°, there will be a global failure. The failure is caused by a strain in which the value equal to the maximum strain failure criteria of the material, namely 0.067. In Figure 3-7, the plastic strain area of the windshield extends as the impact velocity increases (Warsiyanto, Sitompul, et al., 2020). Windshield begins to crack at the upper end at an impact velocity of 67 m/s which is considered as a critical factor. With the same explanation, the plastic strain area of the windshield extends as the bird mass increases as shown in Figure 3-8 (Warsiyanto, Nurrohmad, et al., 2020). Windshield begins to crack at the upper end at a mass of bird 1.13 kg which is considered as a critical factor.

Based on Table 3-1, the greatest energy absorption (internal energy) occurs at an angle -15°, namely 606.17 J. This is due to the more normal angle of impact between the bird and the windshield. The value of the bird kinetic energy and windshield internal energy for impact velocity and mass of bird variations with the same windshield can be seen in (Warsiyanto, Sitompul, et al., 2020) and (Warsiyanto, Nurrohmad, et al., 2020), respectively.

Table 3-1: Kinetic and internal energy maximum of the bird and the windshield, respectively for variations of impact angle

Impact angle (°)	The kinetic energy of the bird (J)	The internal energy of the windshield (J)
15	1736.48	160.12
0		360.76
-8		482.13
-15		606.17

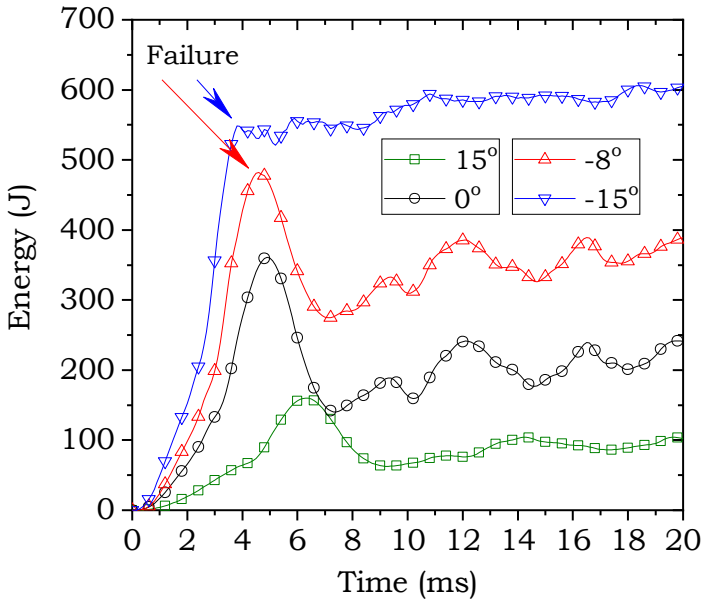

Figure 3-9: Internal energy of the windshield for variations of impact angle

Based on Figure 3-9, the more normal angle of the impact causes an increase in energy absorption by the windshield. Failures begin at angles of -8° at 4.6 ms and -15° at 3.8 ms (marked "Failure" in Figure 3-9) with energy absorption of 482.13 and 548.45 J, respectively. In order to give a simple understanding, Figure 3-10 shows the bird strike process based on time intervals for the curve of the angle of -15°. Table 3-2 shows the change of kinetic energy for the variations of the impact angle with a velocity of 62 m/s and the impact angle of 0°. The largest percentage change in kinetic energy occurs at an angle of -15°, which is 60.64%. In order to obtain the complete and comprehensive knowledge, internal energy of the windshield and changes in the kinetic energy of the bird for impact velocity and mass of bird variations with the same windshield can be seen in (Warsiyanto, Sitompul, et al., 2020) and (Warsiyanto, Nurrohmad, et al., 2020), respectively.

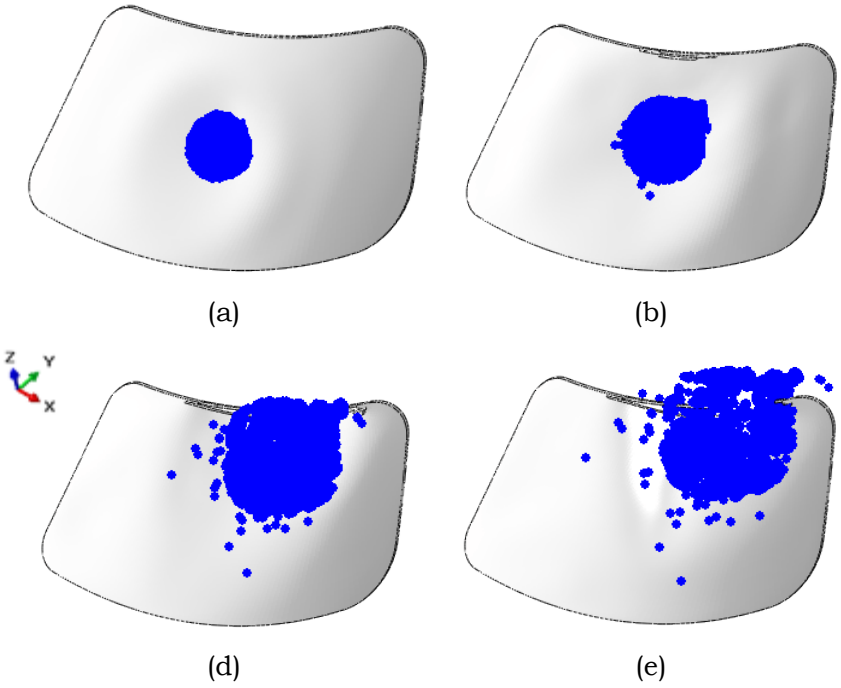

Figure 3-10: Visualization of bird strike simulation for the impact angle of -15° based on time intervals: (a) 2; (b) 3,8; (d) 6; and (f) 10 ms

Table 3-2: Changes in the kinetic energy of the bird before and after impact for angle variations

Impact angle (°)	Kinetic energy (J)		Kinetic energy difference (%)
	Before impact	After impact	
15	1736.48	1444.76	16.80
0		1154.98	33.49
-8		959.49	44.75
-15		683.46	60.64

4. Conclusions

Overall, the impact angle that causes the dynamic response of the windshield in the form of elastic, plastic deformation, and failure in the local area is -8°. This is indicated by the occurrence of failures in the upper end area of the windshield. However, the impact angle that causes the windshield's most dynamic response is -15°. This is indicated by the energy absorption of the windshield that is higher than other impact angles. In addition, the percentage change in kinetic energy before and after the impact is also the largest, namely 37.41%. The upper end of the windshield (fixed) is the weakest part due to the stress concentration which is linearly related to the maximum strain failure criteria of the material.

Acknowledgments

The author would like to thank Mr. Gunawan Setyo Prabowo as Head of the Aviation Technology Center and Mr. Agus Aribowo as Program and Facility coordinator who has supported this research. The author also thanks the LAPAN Aviation Technology Center for the facilities provided in this research.

References

Abaqus. (2014). Analysis User's Guide: Volume II: Analysis. In *ABAQUS 6.14 Analysis User's Guide: Vol. II*.

Dar, U. A., Zhang, W., & Xu, Y. (2013). FE analysis of dynamic response of aircraft windshield against bird impact. *International Journal of Aerospace Engineering*, *2013*. https://doi.org/10.1155/2013/171768

FAA. (2019). *Wildlife Strike Database*. https://wildlife.faa.gov/home

Hedayati, R., Ziaei-Rad, S., Eyvazian, A., & Hamouda, A. M. (2014). Bird strike analysis on a typical helicopter windshield with different lay-ups. *Journal of Mechanical Science and Technology*, *28*(4), 1381–1392. https://doi.org/10.1007/s12206-014-0125-3

Hedayati, Reza, & Sadighi, M. (2015). Bird Strike: An Experimental, Theoretical and Numerical Investigation. In *Woodhead Publishing*. https://doi.org/10.1016/C2014-0-02336-2

Hedayati, Reza, & Ziaei-Rad, S. (2013). A new bird model and the effect of bird geometry in impacts from various orientations. *Aerospace Science and Technology*, *28*, 9–20. https://doi.org/10.1016/j.ast.2012.09.002

Heimbs, S. (2011a). Bird strike simulations on composite aircraft structures. *2011 SIMULIA Customer Conference. Barcelona, Spain*, 1–14. http://www.3ds.com/fileadmin/PRODUCTS/SIMULIA/PDF/scc-papers/Aero-Bird-Strike-Simulations-Composite-Aircraft-Structur.pdf

Heimbs, S. (2011b). Computational Methods for Bird Strike Simulations: A Review. *Computers and Structures*, *89*(23–24), 2093–2112. https://doi.org/10.1016/j.compstruc.2011.08.007

Heimbs, S., Machunze, W., Brand, G., & Schlipf, B. (2015). Bird Strike Analysis for Impact - Resistant Design of Aircraft Wing Krueger Flap. *2015 SIMULIA Community Conference*, 1–11.

Republic Indonesia Ministry of Transportation. (2014). *Civil Aviation Safety Regulation Part 23 amdt1 Airworthiness Standard: Normal, Utility, Acrobatic, and Commuter Category Airplanes*. 1–272.

Shahimi, S. S., Abdullah, N. A., Hrairi, M., & Ahmad, M. I. M. (2021). Numerical Investigation on the Damage of Whirling Engine Blades Subjected to Bird Strike Impact. *Journal of Aeronautics, Astronautics and Aviation*, *53*(2), 193–199. https://doi.org/10.6125/JoAAA.202106_53(2).11

Siemann, M. H., & Ritt, S. A. (2019). Novel particle distributions for SPH bird-strike simulations. *Computer Methods in Applied Mechanics and Engineering*, *343*, 746–766. https://doi.org/10.1016/j.cma.2018.08.044

SIMULIA. (2011). *A Strategy for Bird Strike Simulations using Abaqus / Explicit* (Issue Dassault Systems Online Support Document, Answer ID-4493 (Best Practices for Bird Strike Analysis)).

Wang, F. S., & Yue, Z. F. (2010). Numerical simulation of damage and failure in aircraft windshield structure against bird strike. *Materials and Design*, *31*(2), 687–695. https://doi.org/10.1016/j.matdes.2009.08.029

Wang, X., Feng, Z., Wang, F., & Yue, Z. (2007). Dynamic response analysis of bird strike on aircraft windshield based on damage-modified nonlinear viscoelastic constitutive relation. *Chinese Journal of Aeronautics*, *20*(6), 511–517. https://doi.org/10.1016/S1000-9361(07)60075-2

Warsiyanto, B. A., Nurrohmad, A., Fitriansyah, R., Sitompul, S. A., & Utama, A. B. (2020). Analisis tabrak burung pada windshield pesawat komuter 19 penumpang dengan variasi perbedaan massa burung. *Prosiding Seminar Nasional Ilmu Teknik Dan Aplikasi Industri (SINTA)*, *3*(106), 1–6.

Warsiyanto, B. A., Sitompul, S. A., Yuniarti, E., Fitriansyah, R., & Utama, A. B. (2020). Bird Strike Analysis on 19 Passenger Aircraft Windshield with Different Thickness and Impact Velocity. *Jurnal Teknologi Kedirgantaraan*, *5*(2). https://doi.org/10.35894/jtk.v5i2.5

Wilbeck, J. S. (1978). *Impact Behavior of Low Strength Projectiles. Technical Report AFML-TR-77-134. Air Force Materials Laboratory. Wright-Patterson Air Force Base*, *Ohio*, *45433*, *USA*.

Yuniarti, E., & Sitompul, S. A. (2019). Pengaruh Model Burung Silinder dan Silinder dengan Kedua Ujung Setengah Bola dengan Pemodelan Elemen Hingga Kasus Tabrak Burung. *Jurnal Teknologi Dirgantara*, *17*, 41–56.

Zhu, S., Tong, M., & Wang, Y. (2009). Experiment and numerical simulation of a full-scale aircraft windshield subjected to bird impact. *Collection of Technical Papers - AIAA/ASME/ASCE/AHS/ASC Structures, Structural Dynamics and Materials Conference*, *May*, 1–9.